Extraction of Polysaccharides From Bletilla Striata Using a Modified Low-temperature Method and Evaluation of Their Efficacy Against Alzheimer's Disease

Yi-Wen Lin
National Taiwan University
Chih-Hsiang Fang
China Medical University Hospital
Hung-Hsiang Liao
National Taiwan University
Feng Huei Lin (double@ntu.edu.tw)
National Taiwan University https://orcid.org/0000-0002-2994-6671

Research

Keywords: Alzheimer's disease, Bletilla striata, amyloid-β, oxidative stress, anti-inflammation, aluminum chloride

Posted Date: July 7th, 2021

DOI: https://doi.org/10.21203/rs.3.rs-643976/v1

Abstract

Background: Amyloid-β (Aβ) peptides play a key role in Alzheimer's disease (AD), the most common type of dementia. AD is characterized by progressive cognitive and memory loss accompanied by personality changes. *Bletilla striata*, a traditional Chinese medicine, has been widely used in Eastern Asian countries for alimentary canal damage, ulcer, bleeding, bruises, and burns. in this study, we investigated whether BSP could prevent the ROS from Aβ and the possibility to recover from the disease by memory improvement.

Methods: In this study, a polysaccharide from *Bletilla striata* (BSP) with strong antioxidant and anti-inflammatory properties was extracted following a low-temperature method and tested for its efficacy against AD in vitro using N2a and BV-2 cells and in vivo using AD rats.

Results: The characterization of the extracted BSP for its molecular structure and the functional group demonstrated the efficiency of the modified method to retain its bioactivity. In vitro, BSP reduced ROS levels in N2a cells and the expression levels of inflammatory-related genes in BV-2 cells treated with Aβ fibrils. In vivo, BSP recovered the learning memory, ameliorated the morphological damages in the hippocampus and cortex, and reduced the expression of the β-secretase protein in $AlCl_3$-induced AD rats.

Conclusions: To the best of our knowledge, this is the first study of BSP applicating in AD. Collectively, these findings demonstrated the efficacy of BSP to prevent and alleviate the effects of AD.

Background

Alzheimer's disease (AD), first described in 1906, is the most common type of dementia, accounting for 60–80% of all dementia cases. AD is characterized by progressive cognitive and memory loss accompanied by personality changes [1, 2]. Given the expected increase in the aged population, the prevalence of dementia has been projected to increase to 131 million globally by 2050 [2]. This impending rise in societal aging could have a costly social impact in the coming years.

Several studies have revealed that the initial changes in brain physiology by AD to begin years before perceptible symptoms of dementia being observed [3]. At the initial stages, the brain compensates for the changes enabling the individuals to function normally. However, with the progress in neuronal damages, the brain fails to compensate anymore, and individuals show subtle cognitive decline [4, 5]. AD is generally diagnosed by positron emission tomography (PET) and cerebrospinal fluid (CSF) tests [6] that reveal the elevated amyloid-β (Aβ) depositions, which are believed to be related to pathologic changes in preclinical AD [7]. Furthermore, several biomarkers detecting specific proteins in blood or body fluids, which could be correlated to Aβ deposition, pathologic tau, and neurodegeneration, are also used to uncover the pathological process of AD [8].

Aβ is derived from amyloid precursor protein (APP) by a two-step proteolysis reaction of two enzyme complexes, β-secretase and γ-secretase [9]. It has been reported that the accumulation and aggregation of Aβ leading to the formation of senile plaques in the central nervous system causes progressive cognitive memory loss [10]. Furthermore, Aβ can also increase the levels of reactive oxidative species (ROS), which induce oxidative stress to the neuron cells and cause cytotoxicity [11]. In addition, the senile plaques containing the Aβ peptide have also been shown to induce oxidative stress and chronic neuroinflammation, leading to neurotoxicity, which further accelerates the disease progression [12].

Studies have shown that microglia that secrete neuroprotective growth factors and anti-inflammatory cytokines phagocyte Aβ and release enzymes responsible for Aβ degradation delay the progression of AD by contributing to the clearance of Aβ [13, 14]. Therefore, it is expected that by finding a way to diffuse the oxidative stress and chronic neuroinflammation, might slow down the progression of AD or even stop the accumulation of Aβ. However, despite the availability of several reports and significant efforts of the pharmaceutical industries to understand the mechanism, progression and alleviation, there is no effective therapy available to cure AD or inhibit the progression of AD symptoms significantly [15]. Moreover, the drugs currently used to treat AD–donepezil, galantamine, and rivastigmine–mainly focus on anticholinesterase activity rather than diffuse the ROS and neuroinflammation.

Bletilla striata (Thunb.) Reichb. f. (Orchidaceae), a traditional Chinese medicine, has been widely used in Eastern Asian countries for alimentary canal damage, ulcer, bleeding, bruises, and burns [16]. *B. striata* polysaccharide (BSP) is a water-soluble polysaccharide isolated from *B. striata*. The monosaccharides of BSP are composed of (1→2)-linked α-D-mannopyranose and (1→4)-linked β-D-glucopyranose residues with a ratio of 3:1 [17]. Studies have reported that BSP could scavenge the ROS and inhibit the activation of proinflammatory cytokines, including interleukin 6 (IL-6) and tumor necrosis factor α (TNF-α) in a dose-dependent manner [18]. Therefore, we hypothesized that BSP with strong anti-oxidant and anti-inflammatory properties could be effective in preventing AD.

To test this hypothesis, in this study, we investigated whether BSP could prevent the diffusion of ROS from Aβ in vitro and the possibility to recover from the disease by memory improvement in the $AlCl_3$-induced AD rat model in vivo. Furthermore, here, we employed a new method at low temperature for BSP extraction to ensure the retention of its bioactive properties.

The scheme of the experimental design is shown in Fig. 1.

Methods

Materials. *B. striata* was obtained from Seng Chang Pharmaceutical Co., Ltd., (Taoyuan, Taiwan). $Aβ_{42}$ peptides were synthesized by Gendanio Biotech Inc. (New Taipei City, Taiwan). 2,7-dichlorodihydrofluorescein diacetate (DCFDA) and aluminum chloride were purchased from Sigma Aldrich (St Louis, MO, USA). The RT-PCR primers were synthesized by MDBio Inc. (Taipei, Taiwan). The anti-BACE1 antibody and the Aβ (C-Terminal) antibody were purchased from Merck (Darmstadt,

Germany) and Proteintech (Illinois, USA), respectively. The $A\beta_{42}$ peptides were purchased from ASIA BIOSCIENCE CO., LTD., Taiwan.

BSP Extraction and Purification. In the study, a new method was developed to extract BSP at low temperature by combining the cold extraction method with the vacuum system at 0.5 atm to retain the bioactivity of BSP. Briefly, the as-received *B. striata* was chopped into pieces and ground to dry powder. Then 100 g *B. striata* dry powder was homogenized and dispersed by double distilled water in a low-pressure container at 25 ^{o}C for 4 h. The solution was then centrifuged at 10000 g for 10 min; the supernatant was collected and precipitated by adding 3000 mL 95% (v/v) ethanol and allowed to stand for overnight. Afterward, the solution was filtered using a filter paper, and the precipitate was lyophilized and kept in a desiccator for later use. Subsequently, 100 g extracted dried powder was resuspended in 1800 mL distilled water and then mixed with 600 mL Sevage reagent (n-butanol: chloroform = 1:4); the solution was magnetically stirred overnight. On the next day, the mixture was centrifugated at 6000 rpm for 10 min, and the supernatant was collected and dialyzed using an MWCO-3500 dialyzer (Thermo Scientific™, CA, USA) against double-distilled water to remove n-butanol. The final extract was lyophilized to obtain BSP.

The Characterization of Extracted BSP by Fourier-transform Infrared (FTIR) Spectroscopy and Nuclear Magnetic Resonance (NMR). The FTIR analysis was carried out by mixing 10 mg BSP with KBr at a ratio of 1:9 and then pressing it into a disc in an aluminum ring at10 MPa. After that, the ring was mounted on an FTIR spectrophotometer (Spectrum 100 FTIR Spectrometer, PerkinElmer, USA) at the wavenumber range of 450 to 4000 cm^{-1} and 400 nm/min scanning rate.

The molecular structure of BSP was analyzed by ^{1}H NMR and ^{13}C NMR spectra measurements. BSP was dissolved by Chloroform-d ($CDCl_3$) at a concentration of 50 mg/mL, and then the spectra were recorded on a Bruker ARX-600 instrument (600 MHz, Bruker Co., Ltd. Switzerland).

Preparation of Aβ Fibrils. The $A\beta_{42}$ peptides were dissolved in hexafluoro-2-propanol (HFIP, Oakwood Products, Estill, SC, USA) for monomerization to obtain a final concentration of 1 mM. Then the $A\beta_{42}$-HFIP solution was transferred to Eppendorf tubes in aliquots and kept at 25 ^{o}C to evaporate HFIP, and then stored at −80°C for later use.

Immediately before use, the monomerized $A\beta_{42}$ peptides in Eppendorf tubes were completely resuspended in 5 mM in anhydrous dimethyl sulfoxide (DMSO, catalog number D-2650, Sigma) by pipette mixing, and diluted to 100 μM with DMEM medium addition (Dulbecco's modified Eagle's medium, Sigma). It was homogenized in a shaker at 37°C for 7 days to aggregate into Ab fibrils, the final concentration of Ab fibrils was 100 μM [19, 20].

Measurements of Thioflavin T Fluorescence. Thioflavin T (ThT), a commonly used probe to monitor Ab fibril formation emits fluorescence upon binding to Ab fibrils and the intensity of fluorescence is used to measure the concentration of Ab fibrils. To monitor the aggregation of $A\beta_{42}$ into Ab fibrils, 10 μM $A\beta_{42}$

peptides were added to phosphate-buffered saline (PBS, pH 7.4) at 37°C and transferred onto 96-well plates (Bio-One, Greiner) containing 10 μM ThT. The fluorescence intensity at 485 nm was measured by an ELISA reader (Infinite 200Pro, Tecan) under an excitation wavelength of 440 nm, after 1, 4, 7, 11, and 14 days.

Transmission Electron Microscopy (TEM). A 400-mesh copper grid covered with Formvar and carbon (01754-F) was obtained from Ted Pella, INC, Taiwan. Ten microliters of Aβ42 (10 mM) were dropped onto the copper grids and dried at room temperature. It was then stained with 10 μL 1% (w/v) uranyl acetate (UA) for 20 s. The grid was washed with 10 μL distilled water two times and dried at room temperature. The images of aggregated Ab fibrils at different time intervals (day 7 and day 14) were examined using a transmission electron microscope (TEM, Hitachi H7650) operated at an acceleration voltage of 70 kV.

Evaluation of Cell Viability. The effects of BSP on cell viability were evaluated by the water-soluble tetrazolium (WST-1) assay (TaKaRa, Kusatsu, Shiga, Japan) using the N2a cell lines obtained from Bioresource Collection and Research Center (Hsinchu, Taiwan). The N2a cells were cultured in Dulbecco's modified Eagle's medium (DMEM, Sigma) containing 1% Antibiotic-Antimycotic (Gibco) and 10% Fetal bovine serum (FBS, Hyclone) and incubated at 37 °C and 5% CO_2 in a 95% humidified incubator [21].

The overall process was based on the regulation of ISO 10993-5. Prior to the assessment, first, the extraction solution was obtained by soaking 1 mg/mL BSP in 10 mL culture medium for a day. In addition, the pre-cultured N2a cells were seeded onto 96-well plates with a density of 1×10^4 cells/well and cultured for one day. Subsequently, the extraction solution was added into the culture wells and further cultured for one day. After that, 200 μL WST-1 reagent was added into each well and incubated at 37°C for 2 h. The OD value of each well was determined at 450 nm by using an ELISA plate reader (SpectraMax iD3, Molecular Devices, Inc, USA). The cell viability was calculated using the following formulae:

$$\text{Cell viability } (\%) = \frac{(\text{OD experiment} - \text{OD background}) \times 100}{(\text{OD control} - \text{OD background})}$$

Zinc diethyldithiocarbamate (ZDEC, Sigma-Aldrich) and aluminum oxide (Sigma-Aldrich) were used as positive and negative controls, respectively. The cells cultured only in the fresh medium were used as the control group. The observations were repeated six times (n = 6) in each group.

Evaluation of Cytotoxicity. Cytotoxicity was evaluated using the LIVE/DEAD staining kit (L3224, Invitrogen) according to the manufacturer's instructions. Briefly, 0.2 g BSP and Aβ-BSP were immersed in 1 mL culture medium at 37 °C for 24 h, respectively, and the medium was used as the extracted medium for subsequent experiments. As described earlier, the pre-cultured N2a cells were seeded on a 24-well plate at a density of 2×10^4 cells/well and incubated for 24 h. Afterward, the 100 μL extracted medium was added to each well, followed by the simultaneous addition of 10 μM Aβ fibrils and 1 mg/mL BSP, and cultured for 1 day. Subsequently, 2 μM calcein AM and 4 μM ethidium homodimer-1 (EthD-1) was added

to each well and incubated at 37°C for 30 min to stain the live and dead cells, respectively. Finally, the LIVE/DEAD staining was observed using a fluorescence microscope (IX81, Olympus) at excitation and emission wavelengths of 488 nm and 515 nm, respectively. N2a cells cultured in the extracted medium only were used as the control group. ZDEC and aluminum oxide were used as positive and negative controls, respectively.

Determination of Cellular ROS Generation. The ability of BSP to diffuse ROS induced by Aβ fibrils was measured by a 2',7' –dichlorofluorescin diacetate (DCFDA)-cellular ROS detection assay kit (ab113851, Abcam). In brief, N2a cells were seeded on 96-well plates at a density of 2.5×10^4 cells/well and cultured for 1 day. Afterward, 1 mg/mL BSP and 10 μM Aβ fibrils were added to each well to induce ROS generation. On the next day, the medium was removed and washed with PBS. Subsequently, a culture medium containing 20 μM DCFDA was added to each well and further cultured for 45 min. The fluorescence intensity representing the ROS level induced by Aβ fibrils was detected using a multimode microplate reader (Molecular Devices, SpectraMax i3x, USA). The excitation and emission wavelengths were 495 and 535 nm, respectively.

Gene Expression Analysis. To assess the anti-inflammatory effects of BSP, we analyzed the expression levels of three inflammatory-related genes— tumor necrosis factor-α (TNF-α), interleukin-6 (IL-6) and interleukin-10 (IL-10) — using BV-2 as target cells. The relative expressions of the genes were estimated from three experimental groups—(1) control group: BV-2 cells seeded on 96-well plate with a density of 1×10^5 cells/mL were cultured without any treatment, (2) Aβ group: BV-2 cells at 1×10^5 cells/mL were cultured and treated with 10 μM Aβ fibrils, and (3) Aβ-BSP group: BV-2 cells at 1 × 105 cells/mL were cultured and treated with 1 mg/mL BSP and 10 μM Aβ fibrils.

Total RNA was extracted using Qiazol reagent (Qiagen, Valencia, CA) following the manufacturer's protocol. Random hexamers (Vivantis Inc., California) and reverse transcriptase (Vivantis Cat No: RTPL12) were used for the first-strand cDNA synthesis with the following PCR parameters: 95°C for 3 min (denaturation), 40 cycles of 95°C for 20 s, 60°C for 30 s (annealing), and 72°C for 30 s (elongation). The real-time RT-PCR was performed using the TOOLS 2X SYBR qPCR Mix (Biotools Co., Ltd., Taipei, Taiwan) on a CFX Connect Real-Time PCR Detection System (Bio-Rad, CA, USA). The specific primers (Biotools Co., Ltd., Taipei, Taiwan) used for real-time RT-PCR are shown in Table 1. The changes in expression of the target genes were calculated using glyceraldehyde 3-phosphate dehydrogenase (GAPDH) as an endogenous control.

Table 1. Primers used for gene expression analysis

Name	Sequence
TNF-α- Forward	5’- CATCTTCTCAAAATTCGAGTACAA -3’
TNF-α- Reverse	5’-TGGGAGTAGACAAGGTACAACCC -3’
IL-6- Forward	5’-GGAGCCCACCAAGAACGATAGTCA -3’
IL-6- Reverse	5’-GAAGTAGGGAAGGCCGTGGTT -3’
IL-10- *Forward*	5’-TAAGGCTGGCCACACTTGAG -3’
IL-10- Reverse	5’-GTTTTCAGGGATGAAGCGGC -3’
GAPDH-Forward	5’- TGCTGAGTATGTCGTGGAGTCT -3’
GAPDH-Reverse	5’- AATGGGAGTTGCTGTTGAAGTC -3’

$AlCl_3$-induced AD Rat Model to Develop Alzheimer’s Disease (AD). Eight-week-old Sprague Dawley (SD) male rats were purchased from BioLASCO Taiwan Co., Ltd. (Taipei City, Taiwan). All experiments were carried out in compliance with the National Taiwan University College of Medicine’s Institutional Animal Care and Use Committee (IACUC no. 20130429). We maintained the animals according to the Guide for the Care and Use of Laboratory Animals. The behavioral tests performed were approved by the Animal Ethics Committee of the National Taiwan University Hospital, Taiwan.

AD was induced by intraperitoneal (IP) injection of $AlCl_3$ (7446-70-0, Sigma-Aldrich) (100 mg/mL $AlCl_3$ dissolved in normal saline) three times a week as described in a previous study [22]. The SD rats (n=18) were randomly categorized into 3 groups with 6 rats per group: (1) Control group: rats injected with normal saline, (2) $AlCl_3$ group: rats injected with $AlCl_3$ (100 mg/kg body weight) three times every week and consecutively for eight weeks, (3) $AlCl_3$-BSP group: rats were injected with $AlCl_3$ (100 mg/kg body weight), and then treated with BSP (10 mg/kg/day) by oral administration during the AD induction period. At the end of the experiment (after 8 weeks), the rats were subjected to the Morris Water Maze test to assess their memory and cognitive functions. The blood was collected to assess the hematological parameters, and serological analysis to check the safety. The cortex and hippocampus were harvested after sacrificing the rats using CO_2 for western blotting and histological examination.

Morris Water Maze Test. The Morris water maze was used to assess working and spatial memory retention in the rats following a previous study [23]. Briefly, the circular pool was divided into four quadrants, with a submerged platform placed in one of the quadrants. For each training session, the rat was gently placed in water at a different drop location and allowed to find the submerged platform; the rat was guided toward the platform if it could not find the platform within 2 min. Once the platform was reached, the rat was allowed to stay on it for 30 s. The training was continued in each quadrant for four consecutive days. After four training sessions, the time taken by the rat to reach the escape platform was recorded using the EthoVision software (Noldus Information Technology, Wageningen, Netherlands). The retrieval tests of working and spatial memories were performed as described in a previous study [24]. To

assess the spatial memory, we recorded the time taken (s) by each rat to reach the escape platform from their initial position, whereas working memory was assessed from the time spent (s) by the rat in the same quadrant (maximum 120 s) without the escape platform [25].

Blood Analysis. The safety in vivo would be evaluated by blood element analysis and serological analysis. Blood from the rats was collected by cardiac punctures at the end of the experiment. Serum was obtained by centrifuging the collected blood samples at1500 rpm at 4°C for 15 min. The collected serum samples were stored at −80°C for subsequent analyses. For biochemical tests, alanine aminotransferase (ALT), aspartate aminotransferase (AST), blood urea nitrogen (BUN), and lactate dehydrogenase (LDH) in serum were measured following a previously described method [26]. For hematological parameter analysis, red blood cells (RBC), hemoglobin (HGB), hematocrit (HCT), mean cell volume (MCV), mean corpuscular hemoglobin (MCH), mean corpuscular hemoglobin concentration (MCHC), reticulocytes (RET), platelets (PLT), white blood cells (WBC), neutrophil (NEUT), lymphocytes (LYMPH), monocytes (MONO), eosinophils (EO), and basophils (BASO) were measured. Blood element and serum were measured by the National Taiwan University Veterinary Hospital, Taiwan. Reference: Charles River Laboratories, CD® IGS Rat Model Information Sheet [26, 27].

Western Blotting. The total protein was extracted from hippocampus and cortex tissues of the experimental animals using RIPA lysis buffer (89900, Thermo Fisher, USA) containing a protease inhibitor cocktail. The protein concentration was measured by the Bradford protein assay kit (Z5030028, BioChain Institute Inc., CA USA). The samples were resolved with equal amounts of protein (25 µg) using 12% SDS-PAGE. Three samples from each group were washed, lysed, and equal amounts of protein were separated and transferred onto a polyvinylidene difluoride membrane (Millipore, Burlington, MA, USA), blocked, and incubated with primary antibodies against (Anti-BACE1, cat. no. ab183612; dilution, 1:500, and anti-β-actin, T5168, Sigma-Aldrich; dilution, 1:5000). BACE1 protein was visualized by enhanced chemiluminescence. The band intensity of BACE1 protein was used to evaluate the recovery conditions of rats from AD.

Histological Analysis and Immunohistochemical (IHC) Staining. The cortex and hippocampus harvested from the experimental rats were treated with a series of alcohol and fixed by 4% glutaraldehyde. The specimens were then bisected and embedded in paraffin. Subsequently, the paraffin-embedded tissue blocks were cut into 5 µm thick sections, placed on the glass slides and stained with BACE1 immuno-histochemical anti-body. Hematoxylin and eosin (H&E) stain was used for contrast imaging. The slides were then deparaffinized and rehydrated with 0.1% hydrogen peroxide (Sigma-Aldrich, USA) in PBS solution for 10 min to block the endogenous peroxidases. For retrieval, nonspecific background staining was blocked by 20 µg/mL proteinase K (Sigma-Aldrich, USA) solution. The solution containing the slides was incubated in a humidified chamber at 37 ºC for 20 min. Primary antibody, Aβ [C-Terminal] antibody obtained from 25524-1-AP, Proteintech, was diluted with 1% BSA in a ratio of 1:500 v/v. The diluted primary antibody was then applied to the slides and incubated at 4 ℃ overnight. After incubation, the tissue sections were washed by TBS containing 0.025% Triton-X 100 with gentle agitation. The sections were further incubated in 1% BSA containing goat anti-rabbit HRP IgG secondary antibody at 1: 5000

(v/v) dilution. Finally, the sections were further treated with 3, 3'-diaminobenzidine (DAB, Sigma-Aldrich, USA) substrate solution as an enhancer to reveal more clear colors under the optical microscope.

Statistical Analyses. The data are expressed as mean ± standard deviation (SD). All statistical analyses were done using one-way ANOVA, where the p-values less than 0.05 were considered statistically significant.

Results

Identification of Molecular Structure and Functional Group. In the study, BSP was extracted from *B. striata* at low temperature combined using a vacuum system to retain the bioactivity of BSP.

Figure 2a shows the FTIR pattern of the extracted BSP. The absorption bands at 807 cm^{-1} and 874 cm^{-1} represented α-mannose residues, whereas the sharp absorption at 1022 cm^{-1} indicated a β-glucose residue. The absorption bands at 1372 cm^{-1}, 2906 cm^{-1}, and 3342 cm^{-1} corresponded to the C-O-C of glycosidic linkage, C-H of the 6-carbon ring, and the hydroxyl group (O–H), respectively.

Furthermore, as shown in Figure 2(b), the pattern of ^{1}H NMR of the extracted BSP revealed a chemical shift at δ 4.80 ppm and δ 4.55 ppm, the characteristic peaks for α-mannopyranose and β-glucopyranose, respectively. The signals in the other chemical shifts in the range of 3.3–4.2 ppm corresponded to the non-anomeric ring protons. The ^{13}C NMR pattern of extracted BSP represented the signals at δ 101.1 ppm and δ 103.5 ppm, attributed to $^{\alpha}$-mannopyranose and -glucopyranose, respectively, whereas the chemical shifts found in the range of 70–80 ppm indicated the non-anomeric carbon rings.

The results of ^{1}H NMR and ^{13}C NMR are in agreement with the results of a previous study obtained by fingerprinting analysis [17], suggesting that the molecular structure and functional groups of BSP extracted by the new method proposed in this study were the same as the BSP extracted by the traditional method.

BSP Inhibit Aβ Fibril Formation. As shown in Figure 3a, neither the control nor the PBS only showed any fluorescence, which was increased significantly with time when ThT was incubated with $Aβ_{42}$ and $Aβ_{42}$ mixed with BSP (Aβ-BSP) in PBS at 37 °C as compared to that in PBS only. However, the intensity of the emitted fluorescence was significantly lower with Aβ-BSP treatment than that obtained by $Aβ_{42}$, indicating the inhibitory effects of BSP on Aβ fibril formation or $Aβ_{42}$ aggregation.

Moreover, the TEM imaging data revealed that in the $Aβ_{42}$ (in PBS) treated cells, $Aβ_{42}$ did not aggregate on day 0, whereas a thick Aβ fibril was formed on day 7 (Figure 3b, c). On the contrary, in Aβ-BSP treated cells, the aggregation of $Aβ_{42}$ was comparatively loose with a lesser number of Aβ fibrils than those observed in the $Aβ_{42}$ treated cells on day 7 (Figure 3d). These findings further supported the findings obtained by the ThT assay. Taken together, it can be inferred that BSP effectively inhibits $Aβ_{42}$ aggregation to block the Aβ fibril formation.

Effects of BSP on Aβ-induced Cytotoxicity and Cell Viability. The protective effects of BSP against Aβ-induced cytotoxicity on N2a cells were assessed by LIVE/DEAD staining. As shown in Figure 4, the survivability of the N2a cells treated with BSP and $A\beta_{42}$-BSP were not significantly different from that observed in control (cells grown in culture medium without any treatment). However, the numbers of dead cells in BSP only treated cells were lower than those treated with $A\beta_{42}$-BSP, indicating the cytotoxic effects induced by Aβ fibrils in N2a cells.

Furthermore, the effects of extracted BSP on the viability of N2a cells evaluated by WST-1 assay revealed that neither the extracted BSP alone nor that mixed with $A\beta_{42}$ showed any toxicity to N2a cells compared to the control.

Antioxidant Activity of BSP. The antioxidant ability of extracted BSP was evaluated by DCFDA assay. As shown in Figure 6, the treatment of $A\beta_{42}$ alone significantly increased the ROS level in N2a cells cultured for 1 day than the control that did not receive any treatment ($p<0.05$), whereas that in $A\beta_{42}$ and BSP treated cells did not vary. However, the ROS level in Aβ-BSP treated cells was significantly reduced than those treated with $A\beta_{42}$ alone, indicating the potential of BSP to ameliorate the Aβ-induced increase in ROS levels.

Anti-inflammatory Activity of BSP. As shown in Figure 7, all three inflammatory genes—*TNF-α, IL-6*, and *IL-10*—were downregulated in the BV-2 cells in the Aβ-BSP group than the Aβ group, suggesting the strong anti-inflammatory properties of BSP (Figure 7).

Morris Water Maze Test. As a next step, we evaluated the effects of BSP in vivo. First, we evaluated its effects **on the** working and spatial memory of rats. As shown in Figure 8a, a normal rat with a good memory reached the escape platform following a relatively straight track (Figure 8a), whereas an $AlCl_3$-induced AD rat could not reach the escape platform even after following a complex track. However, the track followed by a BSP-treated AD rat was like that of a normal rat. Furthermore, the findings revealed that the time required by the BSP group did not differ significantly as compared to that required by the control group (Figure 8b). Collectively, these results indicated the potential of BSP to restore memory in AD rats.

Western Blot Analysis. To investigate the Aβ fibril formations in $AlCl_3$-induced rats, cortex and hippocampus were harvested from the brain tissue, and the expression of the β-secretase (BACE1) protein was analyzed by western blotting. As shown in Figure 9, both in the cortex and hippocampus, BACE1 was highly expressed in $AlCl_3$-induced rats, which was downregulated in BSP-treated AD rats. The quantitative values of the band intensities obtained with the ImageJ software are shown in Figure 9b.

Histological Analysis and Immunohistochemical (IHC) Staining. H&E staining was used to assess the effects of BSP on morphological changes of the cells in the cortex and hippocampus of the $AlCl_3$-induced AD rat. As shown in Figure 10, the hippocampal CA1 and cerebral cortex regions in the control group showed normal morphology, wherein the cells from $AlCl_3$-induced AD rats showed clear damage, such as cellular atrophy, shrinkage, necrosis, and pyknosis indicated by heavy stained and dark nuclei (hyperchromatic cells). In addition, large cells due to neuronal swelling and vacuolation were also observed sporadically. On the contrary, the damage was substantially decreased in $AlCl_3$-induced AD rats treated with the extracted BSP, indicating the ameliorating effects of BSP against the damages induced by AlCl3 in AD rats.

As shown in Figure 10b, the dark-brown amyloid plaques were observed in the hippocampus CA1 and cortex of $AlCl_3$-induced rats by BACE1 antibody-positive stain (indicated by the red arrows). However, no plaques were detected in the control rats, whereas they were hardly traced or observed in very light stains in $AlCl_3$-induced AD rats treated with BSP.

Discussion

In this study, the BSP was successfully isolated and purified from the tubers of *B. striata* following a modified extraction method at low temperature that could effectively keep BSP bioactivity and reduce protein loss. We obtained a new polysaccharide with a molecular weight of 2.35×10^5 Da containing mannose, glucose, and galactose in a molar ratio of 9.4:2.6:1.0. The results indicated that the backbone of BSP consisted of (1→4)-linked mannosyl residues and (1→4)-linked glucosyl residues in a molar ratio of 2:1. A monosaccharide composition analysis revealed multiple repetitive sequences. The molecular structure and functional groups of the extracted BSP characterized by NMR and FTIR (Fig. 2) are fully in agreement with that obtained by the traditional method [17]. Furthermore, the extracted BSP demonstrated good survivability (Fig. 4) and no harm to the N2a cells (Fig. 5) in vitro. It also alleviated the damage to the hippocampus and cortex and recovered the neurodegeneration in AlCl3-induced AD rats in vivo.

The present study demonstrating the aggregation of $A\beta_{42}$ into Aβ fibrils in $A\beta_{42}$ in PBS treated cells, which could be because upon binding to the ThT, the Aβ fibrils restricts the rotation of the benzylamine and benzathiole rings of ThT, consequently emitting fluorescence. Furthermore, it has been shown that the deposition of Aβ fibrils as plaques are enriched with the β-sheet structure, which blocks the neurotransmitter transportations, consequently leading to AD [28]. Furthermore, the findings also show that the formation of Aβ fibrils was reduced by treating the cells with BSP, which could be attributed to the inhibition of the aggregation of $A\beta_{42}$ due to the stereo-obstacles.

It has been reported that microglia surrounding the Aβ fibrils form a protective barrier around them, limit further recruitment of Aβ, and release enzymes responsible for Aβ fibril degradation that delay the progression of AD [29]. Furthermore, it has been established that Aβ plays a significant role in inducing and regulating microglial ROS production. Although the breakdown by microglial proteases could enhance the

clearance of Aβ deposits, the clearance rate is relatively slow to diffuse the stress from deposited Aβ fibrils fully, consequently leading to accumulation of the Aβ fibrils over the years that induces ROS and chronic inflammation [30–32]. In addition, the production of ROS by microglial cells and subsequent oxidative stress are strongly implicated in the pathogenesis of AD. The oxidative stress to the surrounding cells subsequently induces chronic inflammation, which might cause further damage to accelerate AD progression and activate the defense cells to secret pro-inflammation factors [32]. As evident from the findings of this study, BSP effectively inhibited the ROS production from the accumulated Aβ fibrils and downregulated the expression of inflammation-related genes in BV-2 cells, indicating the strong antioxidant and anti-inflammatory properties of BSP.

Several studies have shown that aluminum exposure induces AD with strikingly similar clinical and pathological symptoms [33, 34]. For instance, a study has shown that aluminum has been detected in both senile plaques and neurofibrillary tangle-bearing neurons in the brains of AD patients. In addition, neuropathological and neurobehavioral changes resulting in impaired learning ability induced by aluminum exposure are also evident from animal studies. Here, we demonstrated that AD rats lost cognition with increasing escape latency and reducing the percentage of the time spent in the target quadrant, which was recovered by treating the AD rats with the extracted BSP, suggesting the potential efficacy of BSP to ameliorate the working and learning memory impairment induced by $AlCl_3$ in AD rats (Fig. 8).

BACE1 plays a key role in the production of Aβ; the digestion of APP by BACE1 is the first step in the chain reaction of Aβ aggregation, and its gene deletion has been shown to produce mild phenotypes. Several transcription factor-binding sites are located within the BACE1 promoter region, including NF-κB, Sp1, and PPARγ and the regulatory effects at the transcriptional level are probably involved in the expression of BACE1 [35]. Moreover, several groups have reported that BACE1 levels and activity are increased in the AD brain [32,33], indicating that it plays an attractive therapeutic target for AD. Therefore, studies have attempted to identify factors that can suppress BACE1 expression [9]. In this study using an anti-BACE1 monoclonal antibody, we showed that BACE1 levels become elevated in the brains of $AlCl_3$-induced AD rats, which was subsequently reduced in the BSP treated rats suggesting that BSP could be a potential source for the development of BACE1 inhibitor drugs.

Furthermore, the western blot analysis of BACE1 and BACE1-staining supports the efficacy of BSP to alleviate the damages to the hippocampus and cerebral cortex in $AlCl_3$-induced AD rats. The protective effects of BSP against AD could be attributed to its antioxidative and anti-inflammatory effects. The antioxidative effects of BSP are shown to be mediated through the nicotinamide adenine dinucleotide phosphate oxidase 4 (NOX4)/$p22^{phox}$ signaling pathway [18]. Therefore, it is speculated that BSP might be involved in the inhibition of the expression of NOX4 and p22phox, consequently blocking angiotensin II-induced ROS generation. However, further studies are required to delineate the exact underlying mechanism of action of BSP.

♣ LIMITATIONS

To the best of our knowledge, this is the first study of BSP applicating in AD. Although, the protective effects of BSP against AD could be attributed to its antioxidative and anti-inflammatory effects. It still needs more evidence of BSP against AD. The mechanism of action of BSP and the pharmacokinetics of BSP are the critical role of AD prevention. Therefore, further studies are required to delineate the exact underlying mechanism of action of BSP.

Conclusions

In this study, BSP was successfully isolated and purified from dry *B. striata* by a modified extraction method. The molecular structure and characterized functional groups identified and confirmed by NMR and FTIR, respectively, are in agreement with those reported in previous studies. Though studies have shown its antioxidant and anti-inflammatory effects, this study, for the first time, investigated the role of BSP in AD therapy. The findings demonstrated that the extracted BSP could effectively diffuse ROS from the Aβ fibrils and could have good biocompatibility with N2a cell lines, whereas its anti-inflammatory ability was evident in BV-2 cell lines. It also suppresses the expression of BACE1, a prime therapeutic target for the development of drugs to treat AD. Moreover, BSP treatment in AD rats reduced the damage to the hippocampus and cortex and recovered the neurodegeneration induced by $AlCl_3$. Collectively, the findings of this study indicate that BSP could be a potential therapeutic agent in AD treatment.

Abbreviations

Aβ, amyloid-β; AD, Alzheimer's disease; ALT, alanine aminotransferase; APP, amyloid precursor protein; AST, aspartate aminotransferase; BASO, basophils; BSP, *Bletilla striata* polysaccharide; BUN, blood urea nitrogen; CSF, cerebrospinal fluid; DAB, diaminobenzidine; DCFDA, 2,7-dichlorodihydrofluorescein diacetate; DMEM, Dulbecco's modified Eagle's medium; DMSO, dimethyl sulfoxide; EO, eosinophils; FBS, fetal bovine serum; FTIR, Fourier-transform Infrared; H&E, hematoxylin and eosin; HCT, hematocrit; HGB, hemoglobin; IHC, immunohistochemical; IL-6, interleukin 6; IP, intraperitoneal; LDH, lactate dehydrogenase; LYMPH, lymphocytes; MCH, mean corpuscular hemoglobin; MCHC, mean corpuscular hemoglobin concentration; MCV, mean cell volume; MONO, monocytes; NEUT, neutrophil; NMR, nuclear magnetic resonance; PBS, phosphate-buffered saline; PET, positron emission tomography; PLT, platelets; RBC, red blood cells; RET, reticulocytes; ROS, reactive oxidative species; SD, Sprague Dawley; TEM, transmission electron microscopy; ThT, thioflavin T; TNF-α, tumor necrosis factor α; WBC, white blood cells; WST-1, water-soluble tetrazolium; ZDEC, zinc diethyldithiocarbamate.

Declarations

Ethical Approval and Consent to participate

All experiments were carried out in compliance with the National Taiwan University College of Medicine's Institutional Animal Care and Use Committee (IACUC no. 20130429). We maintained the animals according to the Guide for the Care and Use of Laboratory Animals.

Consent for publication

Not applicable

Availability of data and materials

The datasets used and analyzed during the current study are available from the corresponding author on reasonable request.

Competing interests

The authors declare that they have no competing interests.

Funding

This work was supported by the Institute of Biomedical Engineering, National Taiwan University, Taipei, Taiwan, ROC, Ministry of Science and Technology, Taipei, Taiwan, ROC and National Health Research Institutes (109-1901-01-19-07), Taiwan, Republic of China.

Authors' contributions

YWL collected the data, and drafted the manuscript. CHF contributed to the active discussion of the experimental design and performing of the animal study. HHL executed the majority of the experiments. FHL supervised the study, assisted with study conceptualization, and made a substantial contribution to the revision of the manuscript. All authors have read and approved the final submitted manuscript.

Acknowledgements

The authors would like to express their immense gratitude to the Institute of Biomedical Engineering, National Taiwan University, Ministry of Science and Technology and the National Health Research Institutes for their financial support.

Authors' information

[1]Institute of Biomedical Engineering, National Taiwan University, No.1, Sec. 1, Jen-Ai Road, Taipei City 100, Taiwan (R.O.C.). [2]China Medical University Hospital, No. 2, Yu-Der Rd, Taichung City 404332, Taiwan (R.O.C.). [3]Trauma and Emergency Center, China Medical University Hospital, No.2, Xueshi Rd., North Dist., Taichung City 404018, Taiwan (R.O.C.). [4]Division of Biomedical Engineering and Nanomedicine Research, National Health Research Institutes, No. 35, Keyan Road, Zhunan, Miaoli County 35053, Taiwan (R.O.C.).

References

1. Hippius H, Neundörfer G. The discovery of Alzheimer's disease. *Dialogues Clin Neurosci* 2003, *5* (1), 101–108.
2. 2019 Alzheimer's disease facts and figures. *Alzheimer's & Dementia* **2019**, *15* (3), 321–387.
3. Beason-Held LL, Goh JO, An Y, Kraut MA, O'Brien RJ, Ferrucci L, Resnick SM. Changes in Brain Function Occur Years before the Onset of Cognitive Impairment. J Neurosci. 2013;33(46):18008–14.
4. Selkoe DJ, Hardy J. The amyloid hypothesis of Alzheimer's disease at 25 years. EMBO Mol Med. 2016;8(6):595–608.
5. 2018 Alzheimer's disease facts and figures. *Alzheimer's & Dementia* **2018**, *14* (3), 367–429.
6. Jack CR, Bennett DA, Blennow K, Carrillo MC, Feldman HH, Frisoni GB, Hampel H, Jagust WJ, Johnson KA, Knopman DS, Petersen RC, Scheltens P, Sperling RA, Dubois B, A/T/N: An unbiased descriptive classification scheme for Alzheimer disease biomarkers. *Neurology* 2016, *87* (5), 539–547.
7. Ahn HJ, Zamolodchikov D, Cortes-Canteli M, Norris EH, Glickman JF, Strickland S. Alzheimer's disease peptide beta-amyloid interacts with fibrinogen and induces its oligomerization. Proc Natl Acad Sci U S A. 2010;107(50):21812–7.
8. Jack CR, Bennett J, Blennow DA, Carrillo K, Dunn MC, Haeberlein B, Holtzman SB, Jagust DM, Jessen W, Karlawish F, Liu J, Molinuevo E, Montine JL, Phelps T, Rankin C, Rowe KP, Scheltens CC, Siemers P, Snyder E, Sperling HM, Contributors R, NIA-AA Research Framework: Toward a biological definition of Alzheimer's disease. *Alzheimers Dement* 2018, *14* (4), 535–562.
9. Ehehalt R, Keller P, Haass C, Thiele C, Simons K. Amyloidogenic processing of the Alzheimer β-amyloid precursor protein depends on lipid rafts. The Journal of Cell Biology. 2003;160(1):113–23.
10. Castellani RJ, Rolston RK, Smith MA. Alzheimer Disease. Dm-Dis Mon. 2010;56(9):484–546.
11. Butterfield DA, Swomley AM, Sultana R. Amyloid beta-peptide (1–42)-induced oxidative stress in Alzheimer disease: importance in disease pathogenesis and progression. Antioxid Redox Signal. 2013;19(8):823–35.
12. Kinney JW, Bemiller SM, Murtishaw AS, Leisgang AM, Salazar AM, Lamb BT. Inflammation as a central mechanism in Alzheimer's disease. Alzheimer's Dementia: Translational Research Clinical Interventions. 2018;4:575–90.
13. Heneka MT, Carson MJ, El Khoury J, Landreth GE, Brosseron F, Feinstein DL, Jacobs AH, Wyss-Coray T, Vitorica J, Ransohoff RM, Herrup K, Frautschy SA, Finsen B, Brown GC, Verkhratsky A, Yamanaka K, Koistinaho J, Latz E, Halle A, Petzold GC, Town T, Morgan D, Shinohara ML, Perry VH, Holmes C, Bazan NG, Brooks DJ, Hunot S, Joseph B, Deigendesch N, Garaschuk O, Boddeke E, Dinarello CA, Breitner JC, Cole GM, Golenbock DT, Kummer MP. Neuroinflammation in Alzheimer's disease. *The Lancet. Neurology* 2015, *14* (4), 388–405.
14. Solito E, Sastre M. Microglia Function in Alzheimer's Disease. Front Pharmacol. 2012;3:(14).

15. Graham WV, Bonito-Oliva A, Sakmar TP. Update on Alzheimer's Disease Therapy and Prevention Strategies. *Annual Review of Medicine* 2017, *68* (1), 413–430.
16. Wang C, Sun J, Luo Y, Xue W, Diao H, Dong L, Chen J, Zhang J. A polysaccharide isolated from the medicinal herb Bletilla striata induces endothelial cells proliferation and vascular endothelial growth factor expression in vitro. Biotechnol Lett. 2006;28(8):539–43.
17. Wang Y, Liu D, Chen S, Wang Y, Jiang H, Yin H. A new glucomannan from Bletilla striata: Structural and anti-fibrosis effects. Fitoterapia. 2014;92:72–8.
18. Yue L, Wang W, Wang Y, Du T, Shen W, Tang H, Wang Y, Yin H. Bletilla striata polysaccharide inhibits angiotensin II-induced ROS and inflammation via NOX4 and TLR2 pathways. Int J Biol Macromol. 2016;89:376–88.
19. Stine WB, Jungbauer L, Yu C, LaDu MJ, Preparing synthetic Aβ in different aggregation states. In *Alzheimer's Disease and Frontotemporal Dementia*, Springer: 2010; pp 13–32.
20. Klunk WE, Jacob RF, Mason RP. Quantifying amyloid β-peptide (Aβ) aggregation using the Congo Red-Aβ (CR–Aβ) spectrophotometric assay. Anal Biochem. 1999;266(1):66–76.
21. Jackson BV, Yu HS, Buffington A, Hick PP, Nishimura N, Nozaki N, Tokumaru M, Fujiki K, Hayashi K. Exploration of solar photospheric magnetic field data sets using the UCSD tomography. Space Weather. 2016;14(12):1107–24.
22. Abdel-Aal RA, Assi A-AA, Kostandy BB. Rivastigmine reverses aluminum-induced behavioral changes in rats. *European journal of pharmacology* 2011, *659* (2–3), 169–176.
23. Vorhees CV, Williams MT. Morris water maze: procedures for assessing spatial and related forms of learning and memory. Nature protocols. 2006;1(2):848.
24. Morris R. Developments of a water-maze procedure for studying spatial learning in the rat. *Journal of neuroscience methods* 1984, *11* (1), 47–60.
25. Singh NA, Bhardwaj V, Ravi C, Ramesh N, Mandal AKA, Khan ZA. EGCG Nanoparticles Attenuate Aluminum Chloride Induced Neurobehavioral Deficits, Beta Amyloid and Tau Pathology in a Rat Model of Alzheimer's Disease. Front Aging Neurosci. 2018;10:244–4.
26. Baird MF, Graham SM, Baker JS, Bickerstaff GF. Creatine-kinase-and exercise-related muscle damage implications for muscle performance and recovery. *Journal of nutrition and metabolism* 2012, 2012.
27. Carroll MF, Schade DS. A practical approach to hypercalcemia. Am Family Phys. 2003;67(9):1959–66.
28. Frid P, Anisimov SV, Popovic N. Congo red and protein aggregation in neurodegenerative diseases. Brain Res Rev. 2007;53(1):135–60.
29. Brown MR, Radford SE, Hewitt EW. Modulation of β-amyloid fibril formation in Alzheimer's disease by microglia and infection. *Frontiers in molecular neuroscience* 2020, *13*, 228.
30. Schilling T, Eder C. Amyloid-β-induced reactive oxygen species production and priming are differentially regulated by ion channels in microglia. *Journal of cellular physiology* 2011, *226* (12), 3295–3302.

31. Tang Y, Le W. Differential roles of M1 and M2 microglia in neurodegenerative diseases. *Molecular neurobiology* 2016, *53* (2), 1181–1194.
32. Solito E, Sastre M. Microglia function in Alzheimer's disease. *Frontiers in pharmacology* 2012, *3*, 14.
33. Gauthier E, Fortier I, Courchesne F, Pepin P, Mortimer J, Gauvreau D. Aluminum forms in drinking water and risk of Alzheimer's disease. Environmental research. 2000;84(3):234–46.
34. Walton J. An aluminum-based rat model for Alzheimer's disease exhibits oxidative damage, inhibition of PP2A activity, hyperphosphorylated tau, and granulovacuolar degeneration. J Inorg Biochem. 2007;101(9):1275–84.
35. Rossner S, Sastre M, Bourne K, Lichtenthaler SF. Transcriptional and translational regulation of BACE1 expression–implications for Alzheimer's disease. Prog Neurobiol. 2006;79(2):95–111.

Figures

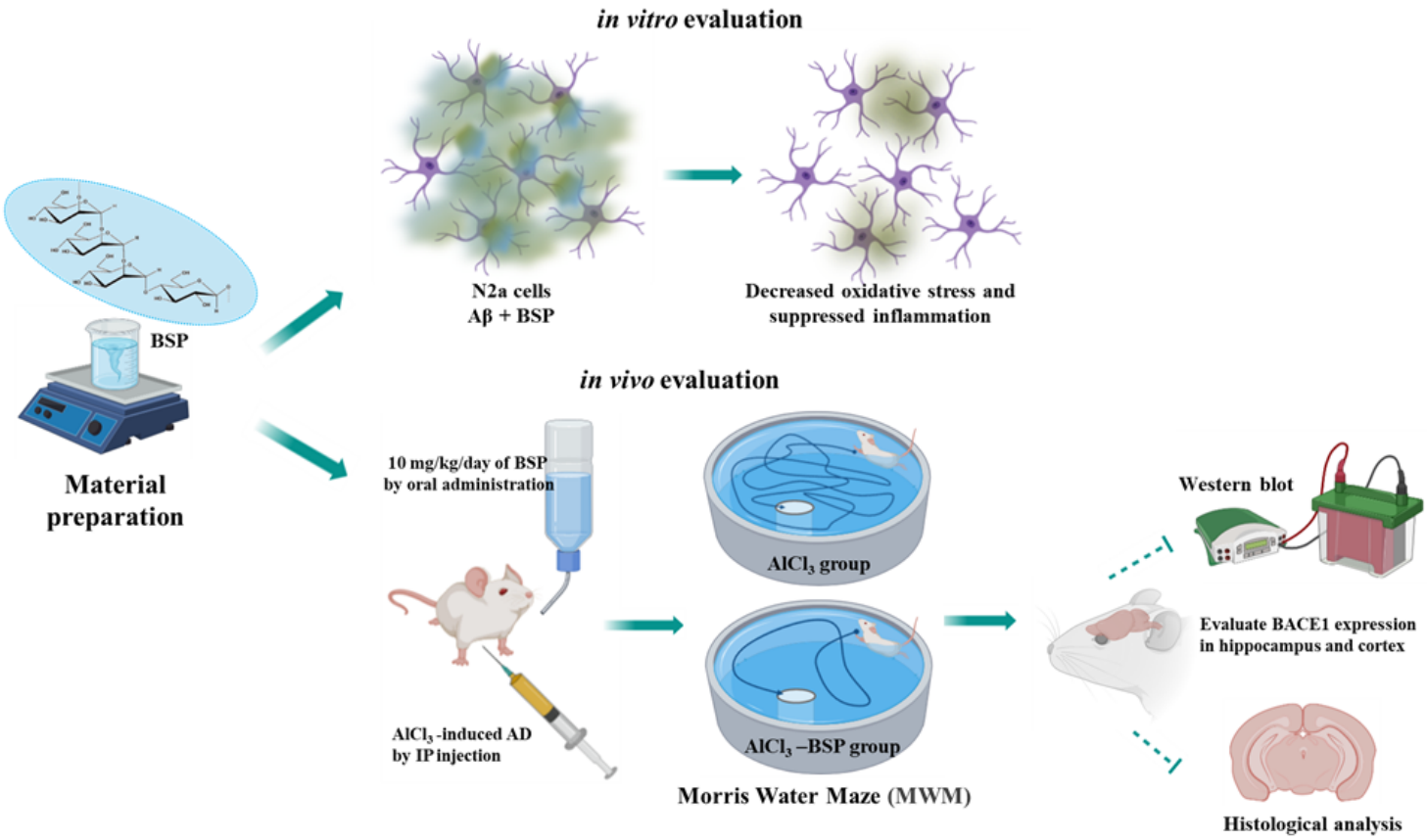

Figure 1

The scheme of the experimental design.

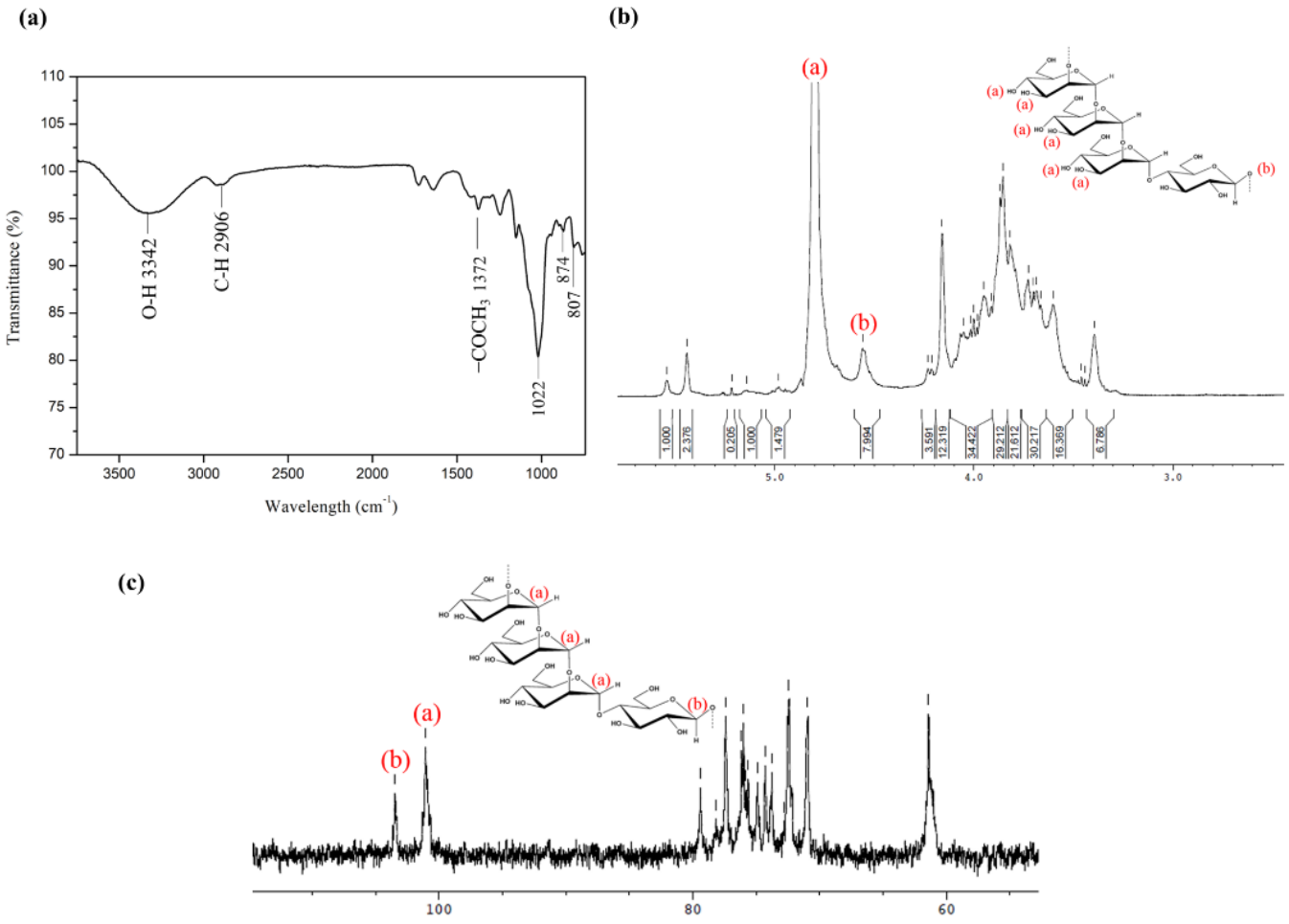

Figure 2

Characterization of extracted BSP. (a) FTIR spectrum; (b) 1H NMR spectrum; (c) 13C NMR spectrum. Those were fully matched to the BSP extracted by the traditional method.

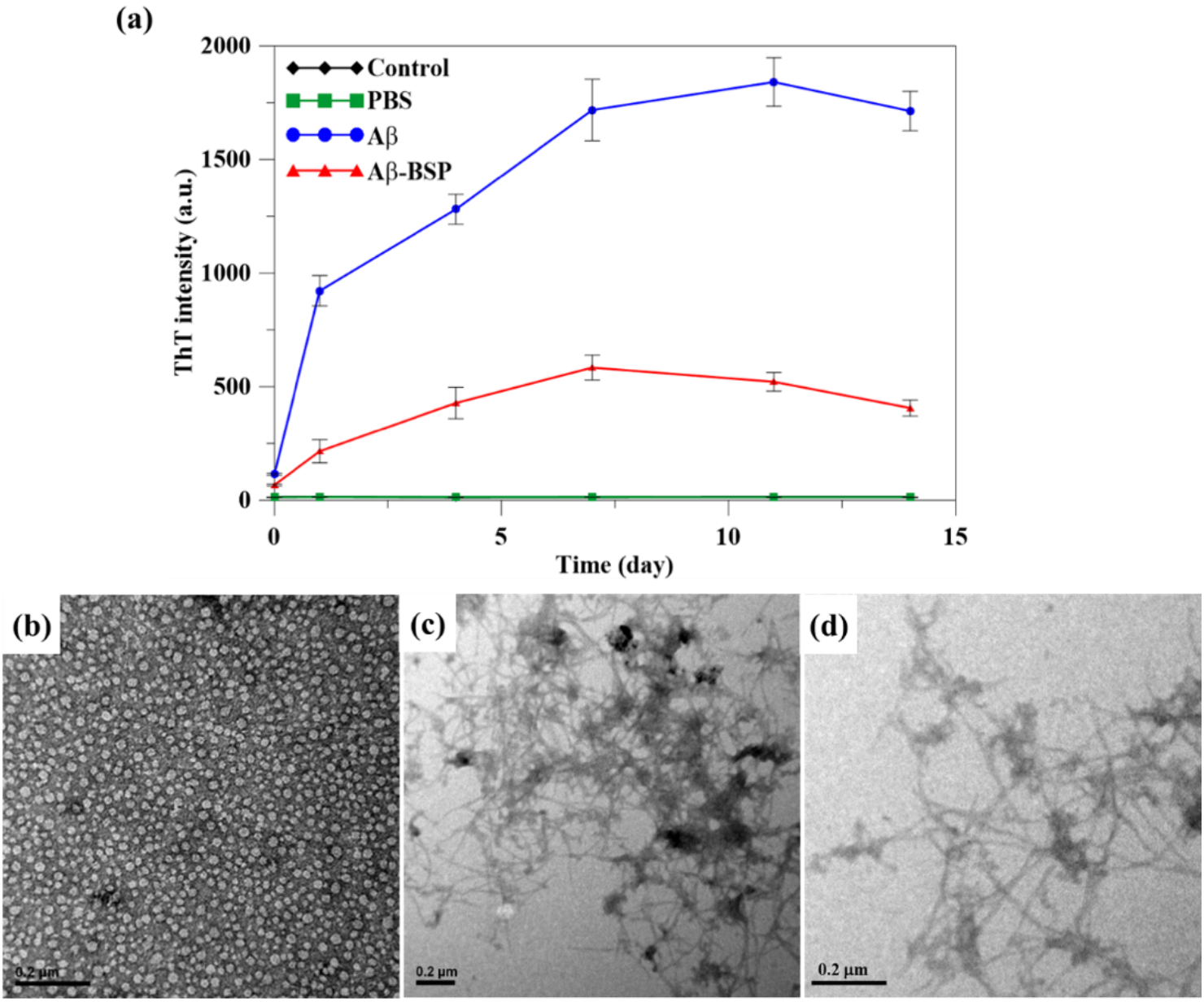

Figure 3

The aggregation of Aβ42 into Aβ fibrils. (a) The fluorescence intensity of ThT obtained by incubation of Aβ42 (Aβ; blue line), Aβ42 mixed with BSP (Aβ-BSP; red line) in PBS at 37 °C for 14 days. The green line represents the fluorescence intensity of ThT in PBS only (PBS). (b) The TEM image of Aβ42 monomers without aggregation on day 0; (c) the Aβ42 aggregated into thick and compact Aβ fibrils on day 7; (d) BSP reduced aggregation of Aβ42 with reduced thickness and loose packing of Aβ fibrils on day 7. The scale bar is 0.2 μm.

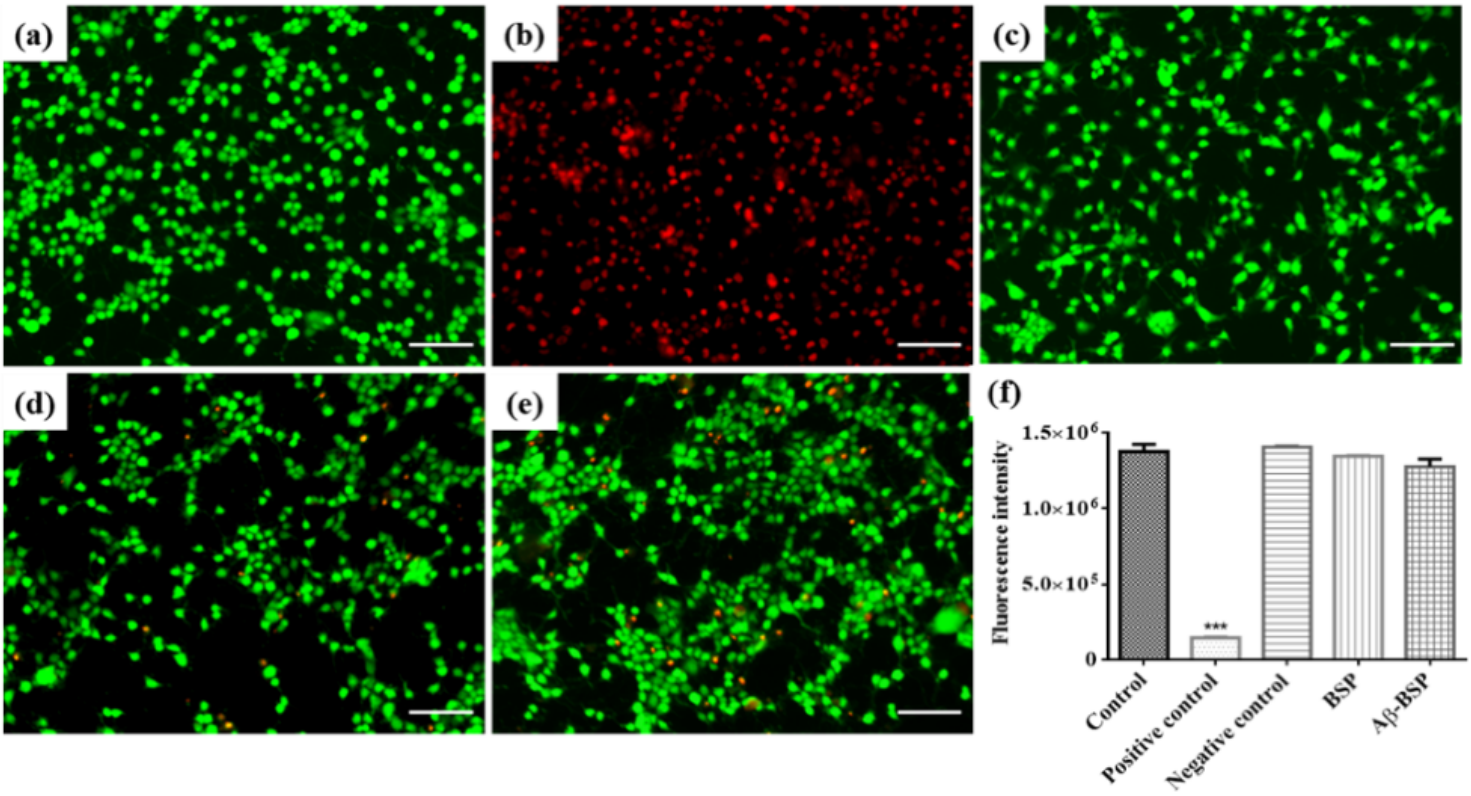

Figure 4

The LIVE/DEAD staining of N2a cells in (a) the control: cells cultured in medium only, (b) positive control: cells treated with Zinc diethyldithiocarbamate, (c) negative control: cells treated with aluminum oxide, (d) BSP: cells treated with an extracted solution of BSP, and (e) Aβ-BSP: cells treated with Aβ42 and BSP. (f) Quantitative results of survival rate in N2a cells. ***P < 0.001 compared with Control.

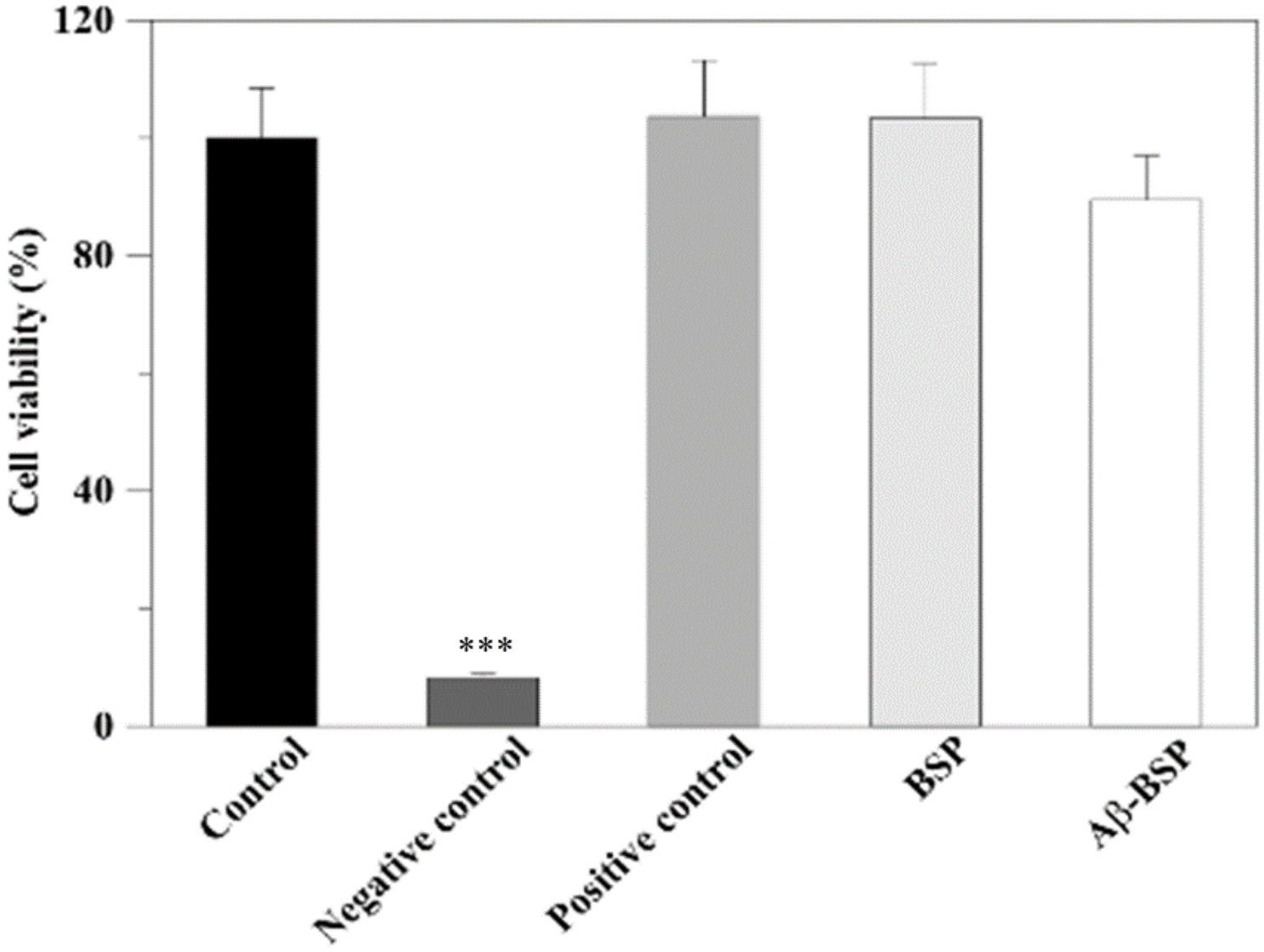

Figure 5

The effects of the extracted BSP on cell viability estimated by the WST-1 assay. (n = 6, ***P < 0.001 compared with control). The abbreviations are as defined in Figure 4.

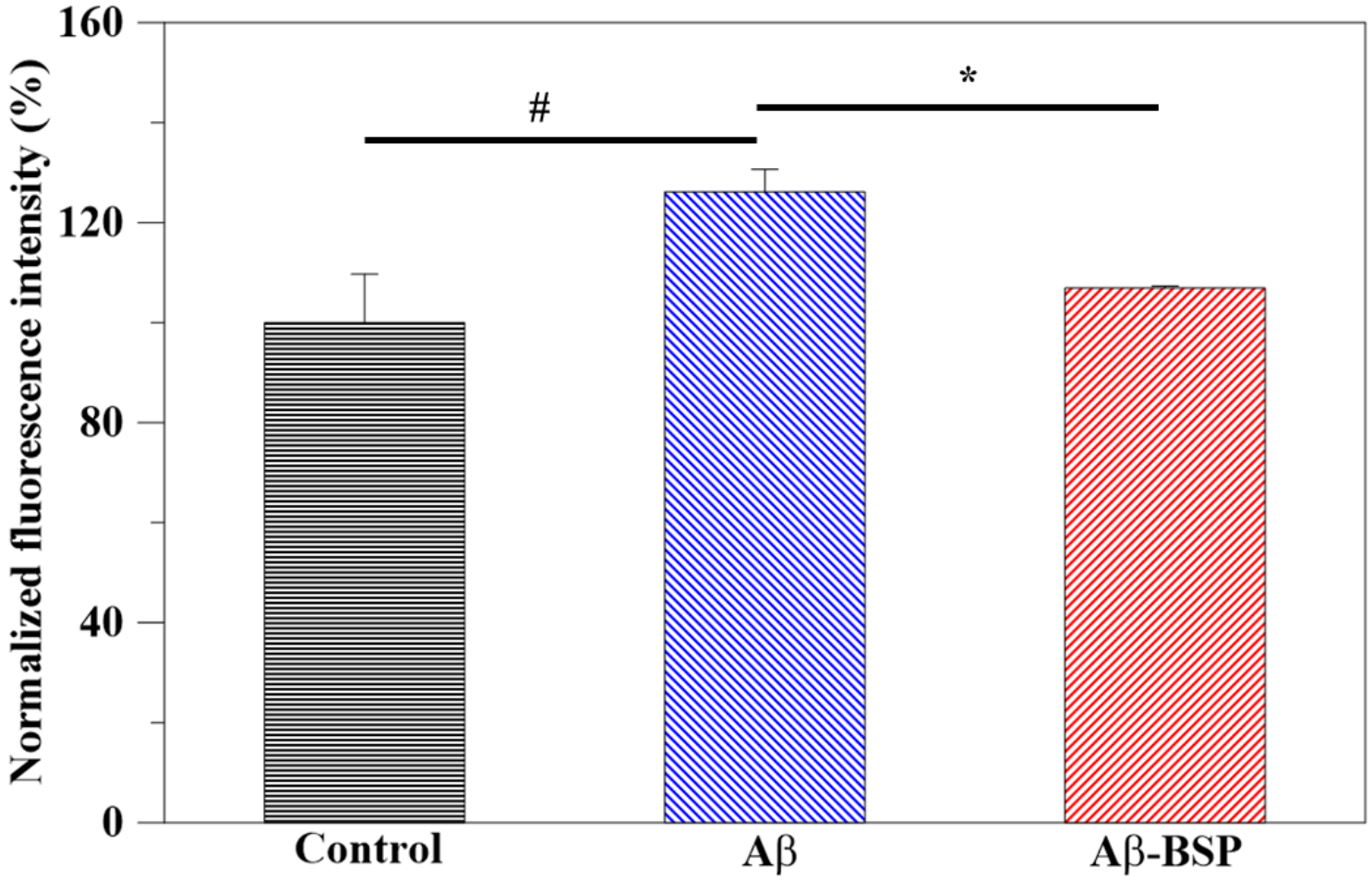

Figure 6

Antioxidant activity of extracted BSP. DCFDA was used to measure the intracellular ROS in N2a cells without any treatment (control), treated with Aβ42 (Aβ), and Aβ42 and BSP (Aβ42-BSP). (n = 6, #p < 0.05 compared to control group, *p < 0.05 compared to Aβ group).

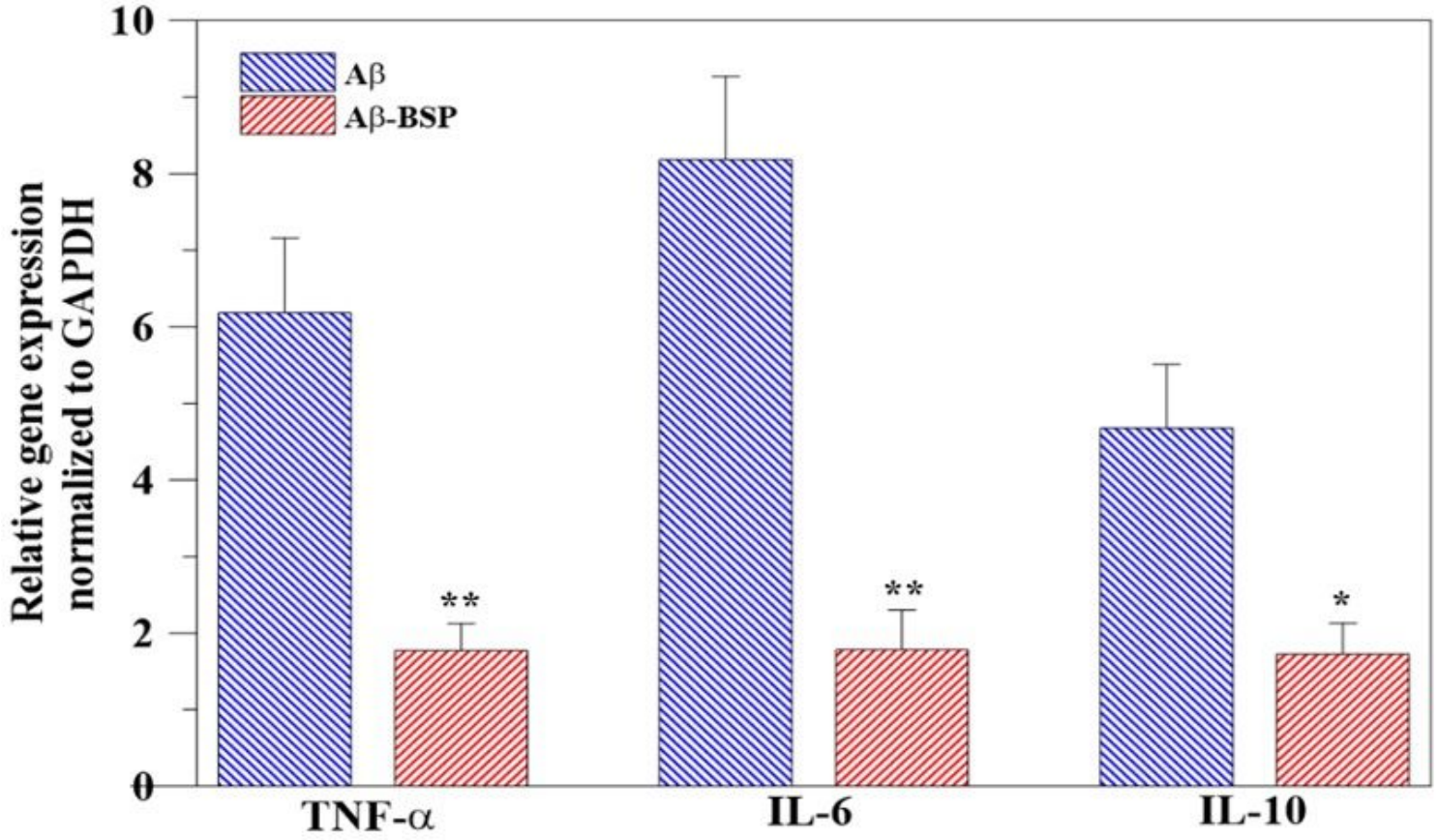

Figure 7

Anti-inflammatory effect of the extracted BSP on Aβ-induced inflammation in BV-2 cells estimated by the expression analysis of inflammation related genes, TNF-α, IL-6, and IL-10. (n = 6, *p < 0.05 compared to Aβ group, **p < 0.01 compared to Aβ group).

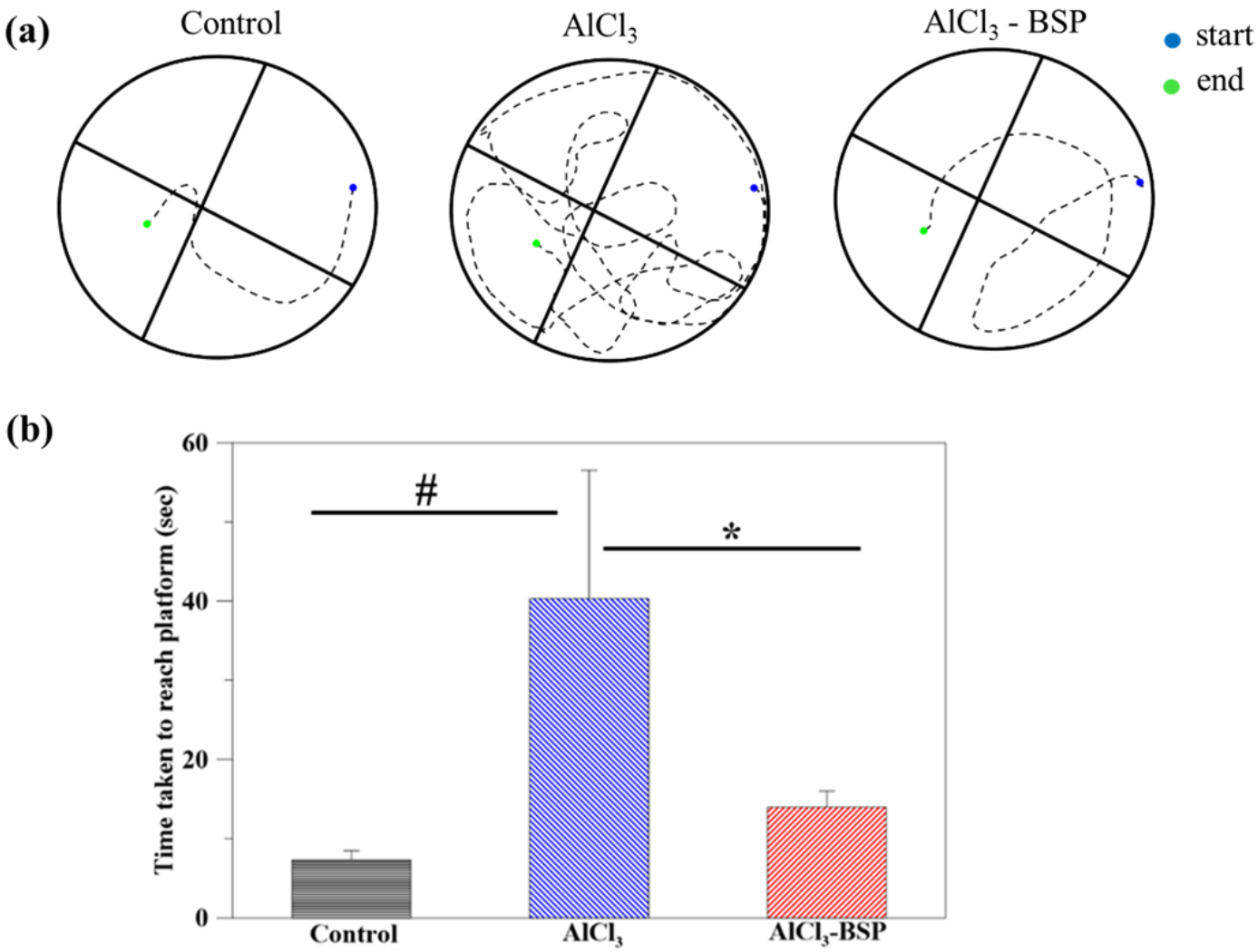

Figure 8

The MWM track of the normal rats (Control), AlCl3-induced AD rats (AlCl3), and BSP-treated AD rats (AlCl3-BSP). The starting point (blue) to endpoint (green) of all the tested rats were the same. (b) The time taken by the tested rats from starting point to reach the escape platform (n = 6 per group, #p < 0.05 compared to control group, *p < 0.05 compared to AlCl3 group).

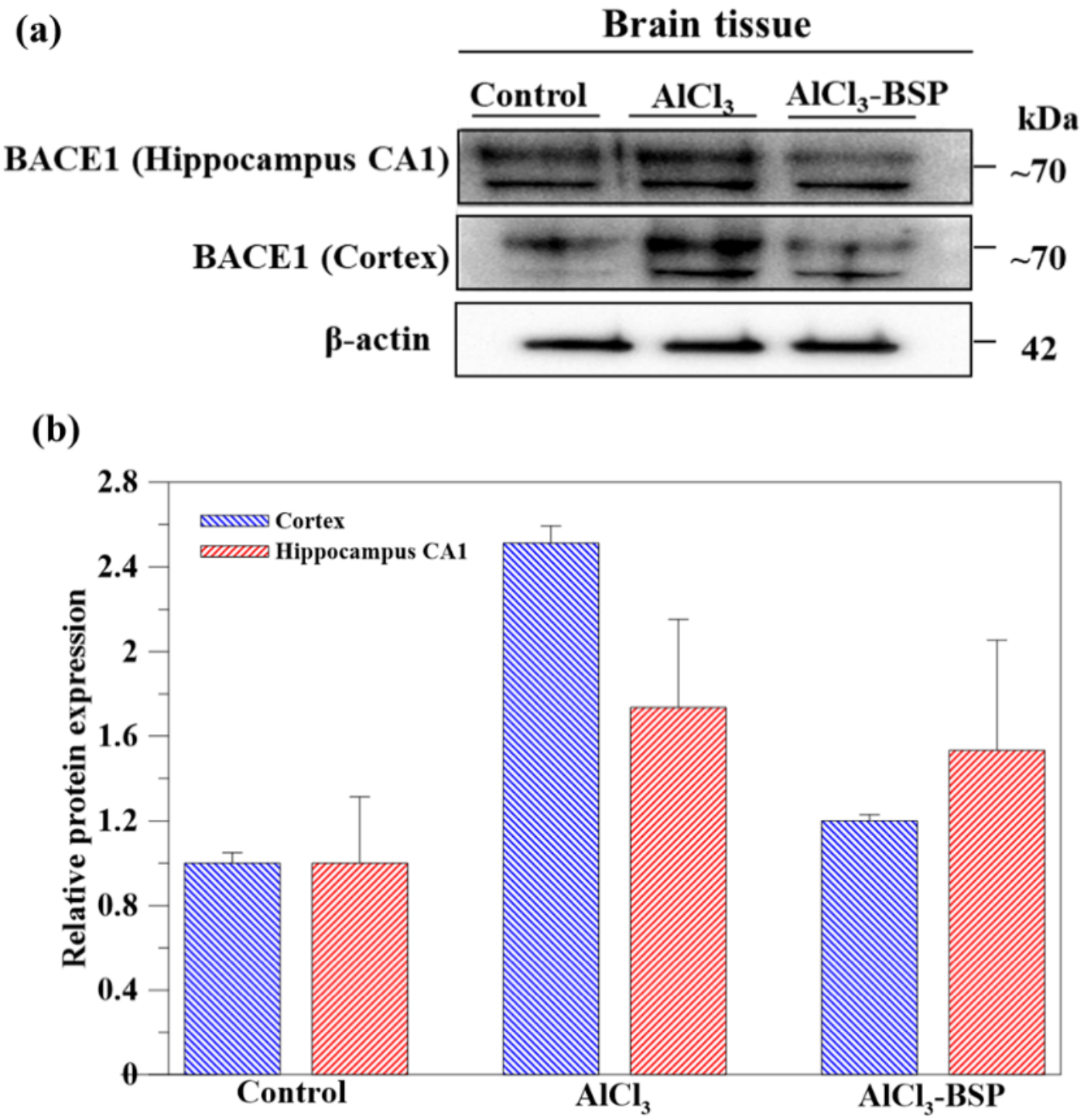

Figure 9

(a) The western blot analysis of BACE1 in Hippocampus CA1 and Cortex. β-actin was used as the loading control. (b) The quantitative values of the BACE1expression data obtained the ratio of BACE1 protein/Actin protein band intensities normalized to 1 in the control group.

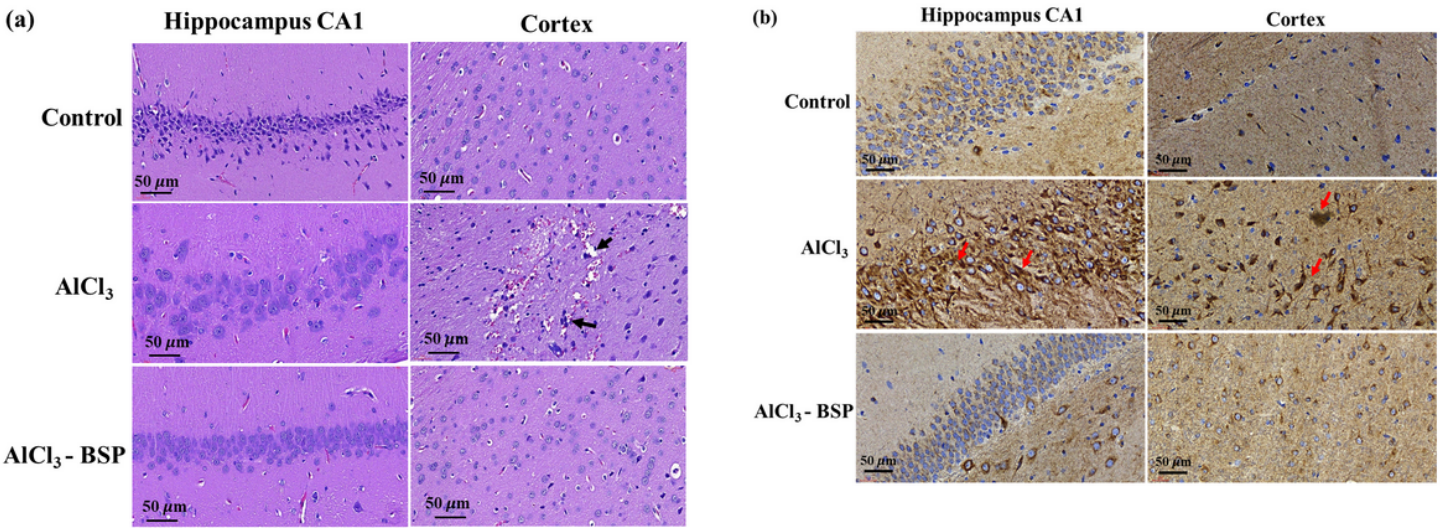

Figure 10

(a) Hematoxylin and eosin (H&E) of Hippocampal CA1 and Cortex regions of the tested rats. Brain sections from rats treated with AlCl3 show that pyramidal cells in the Hippocampal CA1 region exhibit more severe morphological changes. (b) BACE1 reveals plaque-like staining in the brains of AD rats by immunohistochemistry. Brain sections from control rats stained with BACE1 show the normal BACE1 immunoreactivity pattern, whereas those from AlCl3-induced rats display plaque-like BACE1 immunoreactivity, which was reduced in BSP-treated AD rats. Arrowheads indicate plaque-like BACE1-immunopositive deposits. Scale bars: 50 μm.